Friction and Disturbance Compensation for Free-form Contour Following Tasks of Biaxial Linear Motor Systems

Ke-Han Su, Ming-Yang Cheng, Yu-Chen Chang

Department of Electrical Engineering,
National Cheng Kung University, Taiwan

E-mail :mycheng@mail.ncku.edu.tw

Abstract –In modern high-precision machining applications, how to effectively reduce contour error is one of the most important issues concerning multi-axis contour following tasks. Among many existing approaches, the Cross-Coupled Controller (CCC) is widely used in contour following tasks to improve contouring accuracy. However, when a servomechanism is operated in reverse or low-speed motions, the performance of the CCC will be degraded because of inherent friction force and external disturbance. Therefore, to cope with the aforementioned problems, this paper exploits the Karnopp friction model-based compensator and the Virtual Plant Disturbance Compensator (VPDC) to improve tracking performance as well as contouring accuracy. Moreover, to further improve contouring performance, an integrated motion control scheme is also developed. The proposed scheme consists of two position loop controllers with velocity command feedforward, a modified CCC, two friction force compensators, and two disturbance compensators. In order to evaluate the performance of the proposed approach, several free-form contour following experiments have been conducted on an X-Y table driven by two linear motors. Experimental results verify that the proposed approach can significantly enhance contouring performance for free-form contour following tasks.

Keywords - *Contour error, Cross-Coupled Controller, friction force, disturbance compensator.*

I. INTRODUCTION

In multi-axis motion control applications, the machining error consists of position error (tracking error) and contour error (as indicated in Fig.1.). Generally, the contour error represents a better indication of precision than tracking error in high-precision machining. Consequently, how to effectively reduce contour error is one of the most important issues concerning multi-axis free-form contour following tasks.
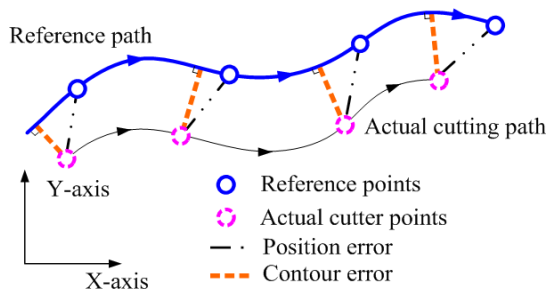

Fig. 1. Schematic diagram of the position and contour errors for a free-form contour following task in a biaxial motion control system.

In addition to using the conventional feedback control scheme, there are many approaches that focus on developing different control strategies for contouring accuracy improvements. For instance, some researchers exploit the idea of command feedforward control to improve tracking performance of each individual axis so that the contour error of a multi-axis contour following task can be reduced as well [1, 2]. Moreover, to further reduce contour error in a multi-axis contour following task, Koren proposed the Cross-Coupled Control (CCC) structure [3]. Recently, the CCC has become one of the most popular and widely used approaches for contour error reduction of multi-axis contour following tasks [4-9]. However, when a servomechanism is operated in reverse or low-speed motions, the performance of the aforementioned approaches may deteriorate because of inherent friction force or external disturbance. The situation becomes even worse when performing a relatively complex free-form curve or surface machining task (i.e. a command trajectory has different radius of curvatures).

To deal with the aforementioned problems, several investigations of different types of friction force and disturbance compensation approaches have been recently developed [8-15]. For instance, according to the Coulomb friction-model, Yan et al. [8] proposed a self-tuning adaptive control scheme for friction effects suppression so as to improve contouring accuracy. Tsai et al. [10] exploited a Kranopp friction-model-based feedforward compensator to eliminate stick-slip friction effects in a biaxial contouring control system. In addition, rather than using friction-model-based approaches, Jee and Koren [11] proposed a self-organizing fuzzy logic control for friction force compensation in 3-axis contour milling tasks. On the other hand, to cope with external disturbances such as external load torque or cutting force, many researchers employ the disturbance observer (DOB) [12] in contouring control problems. For example, Yan and Shiu [13] exploited a discrete-time DOB [9] to help improve the contouring accuracy for wire-EDM machine contour machining. Moreover, to further enhance the tracking performance and therefore reduce contour error, some investigators use both friction and disturbance compensation approaches simultaneously in contour following tasks (e.g. Yeh et al. [9], Jamaludin et al. [14], and Jee and Tomizuka [15]). This paper employs a similar approach to achieve better machining accuracy for biaxial motion control systems. In particular, this paper exploits a feedforward friction force compensator (based on the Kranopp friction-model [16]) and the Virtual Plant Disturbance Compensator [17] to suppress the large machining errors caused by the unknown system uncertainties and nonlinearities such as friction force

or external disturbances.

The rest of the paper is organized as follows. Section 2 provides a brief introduction to the Karnopp friction-model and the VPDC. The integrated motion control scheme developed in this paper is presented in Section 3. Section 4 includes the experimental setup and results. Finally, the conclusions are drawn in Section 5.

II. FRICTION AND DISTURBANCE COMPENSATION FOR MOTION CONTROL SYSTEMS

How to suppress the adverse effects due to friction and disturbance are crucial and challenging in precision motion control problems. In particular, when a servomechanism undergoes a low-speed motion, the friction force may result in a stick-slip phenomenon that will degrade the motion accuracy. To cope with this problem, one of the popular approaches is to develop a friction model based feedforward compensator. On the other hand, to deal with the issues such as external disturbance or parameter variation/uncertainty, the disturbance observer (DOB) is one of the most popular and easily implemented approaches in motion control problems. Generally, the idea of disturbance observer is to treat all the system uncertainties and nonlinearities (including the friction force and external load torque) as an external disturbance, and then further compensate for it. Over the past decades, different types of DOB have been widely used to suppress the adverse effects caused by the external disturbance and friction force. However, in most situations, the disturbance observer may not able to effectively deal with the adverse effects due to nonlinear disturbance such as friction force. Consequently, in order to cope with the aforementioned problem, this paper develops a Karnopp friction-model based feedforward compensator. Additionally, a disturbance compensation scheme VPDC is also exploited to suppress external disturbance. Fig. 2 illustrates the overall schematic diagram of a speed control system combined with the Karnopp friction-model feedforward compensator and the disturbance compensator VPDC. Brief introductions to the Karnopp friction-model and the VPDC are given in the following.

A. Brief Introduction to the Karnopp Friction-model

To account for the friction phenomenon around near-zero velocity motions, Karnopp proposed an alternative approach to construct the friction-model [16]. Fig .3 is the schematic diagram of the Karnopp friction-model. This friction-model describes two different friction functions for stick and slip behaviors, which are established according to a specified velocity interval $\pm DV$. As shown in Fig. 3, if the relative velocity between two contact surfaces is smaller than the specified velocity interval $|\pm DV|$ (i.e. in the stick state), the friction force will be equal to the external force F_E and limited to the break-free force F_H. In contrast, if the relative velocity between two contact surfaces exceeds to the specified velocity $|\pm DV|$ (i.e. in the slip state and exceeds the break-free force F_H), the friction force will be determined by a friction function $f(v)$ which consists of Coulomb and viscous friction. The Karnopp friction-model is expressed as:

$$F_{fric} = \begin{cases} \min(F_H, F_E) \cdot sgn(v), & |\pm v| \le DV \\ f(v) = (F_c + F_v \cdot |v|) \cdot sgn(v), & \text{otherwise}. \end{cases} \quad (1)$$

where v is the relative velocity between two contact surfaces, F_c is the Coulomb friction coefficient and F_v is the viscous friction coefficient.

B. Brief Introduction to the VPDC[17]

The VPDC has shown excellent ability in suppressing external disturbance [17]. Compared with the existing disturbance observer [18], the advantage of VPDC is that it not only can accurately estimate the disturbance load torque, but also has better capability in suppressing external load disturbance. Therefore, in addition to using the friction force compensator, this paper further exploits the VPDC to improve contouring accuracy.

Fig. 4 illustrates the block diagram of a speed control system with the VPDC. In Fig. 4, $1/(J_m s + B_m)$ represents the real transfer function of the plant under control, while $1/(\hat{J}_m s + \hat{B}_m)$ represents the reference plant model obtained through system identification. Note that in Fig. 4, T_m, T_d, and $\hat{T}_d$ are the torque command, real disturbance load torque, and the load torque estimated from the VPDC. ω_{cmd}, ω, and $\hat{\omega}$ are the velocity command, estimated velocity of the real plant and the identified reference model, respectively. In addition, Kv_p and Kv_I are the proportional gain and integral gain of the velocity loop controller, while K_1 and K_2 are the gain constants used to adjust the pole position of the disturbance observer. The analysis of disturbance estimation ability of the VPDC is provided in the following.

By using the Mason's gain formula, the transfer function from the torque command to the estimated load torque in Fig.4 can be described by (2) and (3), respectively.

$$\frac{\hat{T}_d(s)}{T_m(s)} = \frac{(K_1 s + K_2)(J_m s - \hat{J}_m s + B_m - \hat{B}_m)}{(\hat{J}_m s + \hat{B}_m)((J_m s + B_m)s + (K_1 s + K_2))}; \quad (2)$$

$$\frac{\hat{T}_d(s)}{T_d(s)} = \frac{(K_1 s + K_2)}{(J_m s + B_m)s + (K_1 s + K_2)}. \quad (3)$$

To simplify the analysis, without loss of generality, the torque command and load torque are set to constant values in the following derivations. That is, $T_m(s)=C_m/s$, $T_d(s)=C_d/s$, where C_m and C_d are constant. Therefore, the overall estimated load torque in the steady state ($s \to 0$) can be rewritten as:

$$\tilde{T}_{dss} = \frac{\hat{T}_d}{T_m} + \frac{\hat{T}_d}{T_d} = \frac{K_2(B_m - \hat{B}_m)}{B_m K_2} \times C_m + \frac{\hat{B}_m K_2}{B_m K_2} \times C_d. \quad (4)$$

If the identified reference model is accurate enough (i.e. $\hat{B}_m \cong B_m$), (4) can be simplified as $\tilde{T}_{dss} \cong C_d$. It indicates that the estimated load torque obtained using the VPDC is equal to the real load torque. The above theoretical analysis suggests that the VPDC can provide accurate disturbance estimation when used to suppress disturbance in motion control systems. For more details about the VPDC, please refer Ref. [17].
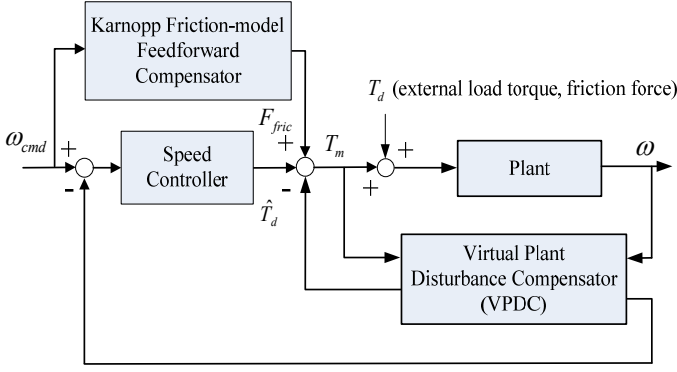
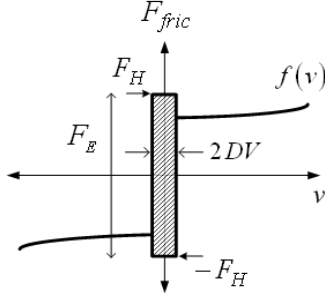Fig. 2. Block diagram of a speed control system combined with friction and disturbance compensators.

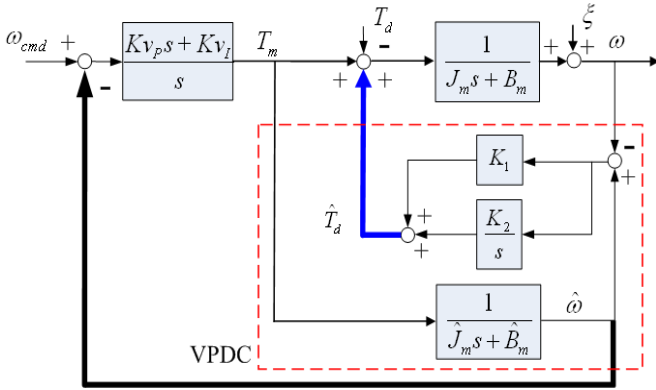
Fig.3. Karnopp friction-model [16].

Fig. 4. Block diagram of a speed control system with the VPDC [17].

III. THE PROPOSED INTEGRATED MOTION CONTROL STRUCTURE

It is a trend that modern CNC machine tools must be capable of high-precision and complex curve/surface machining operations to achieve both the goals of high accuracy and performance in free-form contour following applications. To achieve such a goal, in this paper an integrated motion control scheme consisting of two position loop controllers with the velocity command feedforward, a modified CCC (equipped with a real-time contour error estimator), two feedforward friction compensators, and two VPDC is proposed.

In the integrated motion control scheme, the modified CCC is applied to reduce the contour error for free-form contour following tasks, while others are employed to further improve the tracking performance of each individual axis so that the contour error can also be reduced as well. In

particular, the feedforward friction compensator and the disturbance compensator are exploited to suppress the adverse effects due to system uncertainties or nonlinearities for each axis. Fig. 5 shows the schematic diagram of the motion control structure proposed in this paper, where K_c is the cross coupled controller, E'_c is the estimated contour error, C_x, C_y are the cross-coupled gains, K_{fx} and K_{fy} are the feedforward loop controllers, K_{px} and K_{py} are the position loop controllers, PI_{vx} and PI_{vy} are the velocity loop controllers. E_x, E_y are the tracking errors of the system. ω_{cx}, ω_{cy} and ω_x, ω_y are the input velocity command and output velocity of each axis. R_x, R_y and P_x, P_y are the reference command positions and actual positions, respectively. In particular, the values of C_x, C_y are set to $-\sin\phi$ and $\cos\phi$, respectively. Note that ϕ is the angle between the straight line path and the X-axis, which is defined in Ref. [19].

IV. EXPERIMENTAL SETUP AND RESULTS

Several free-form contour following experiments are conducted so as to evaluate the performance of the proposed approach.

A. Experimental Setup and System Parameter

The experimental system hardware and parameter settings are presented in the following.

1) Hardware of the Experimental System: In this paper, an X-Y table system is employed as a test platform to evaluate the performance of the proposed approach. The linear X-Y table system consists of an X-Y table, a personal computer, and a PC-based motion control card (ITRI IMP-2). The X-Y table is driven by two HIWIN linear motors that are equipped with the Copley Controls servomotor drives. In addition, two linear optical encoders with a resolution of 1 μm are used to measure the tracking error of each axis. Moreover, the drives for both linear servomotors are set to the torque mode throughout the experiments. Note that the sampling period is set to 1 ms in this paper. A photograph of the experimental hardware is presented in Fig. 6.

2) Parameter Setting of Motion Control System: The parameters of the transfer functions for both the motions in the X-axis and Y-axis are obtained using the system identification approach proposed by Johnson and Lorenz [20]. Based on the obtained model parameters, one can determine appropriate gain constants for the proposed integrated motion control scheme illustrated in Fig. 5. The identified model parameters and the selected gain constants for the experiment are summarized in Table I. In addition, the reference command positions R_x, R_y are generated by a real-time Non-uniform Rational B-spline (NURBS) interpolator [21]. Moreover, according to the measured friction information, the Karnopp friction-models for both axes are described by (5) and (6). Note that the specified velocity interval $\pm DV$ in (1) is set to ± 1mm/s in the this paper.

$$Fx_{fric}(v) = \begin{cases} 7\times10^{-4}v + 0.4423, & \text{for } v > 1\text{mm/s} \\ 8\times10^{-4}v - 0.4091, & \text{for } v < -1\text{mm/s} \end{cases} \quad (5)$$
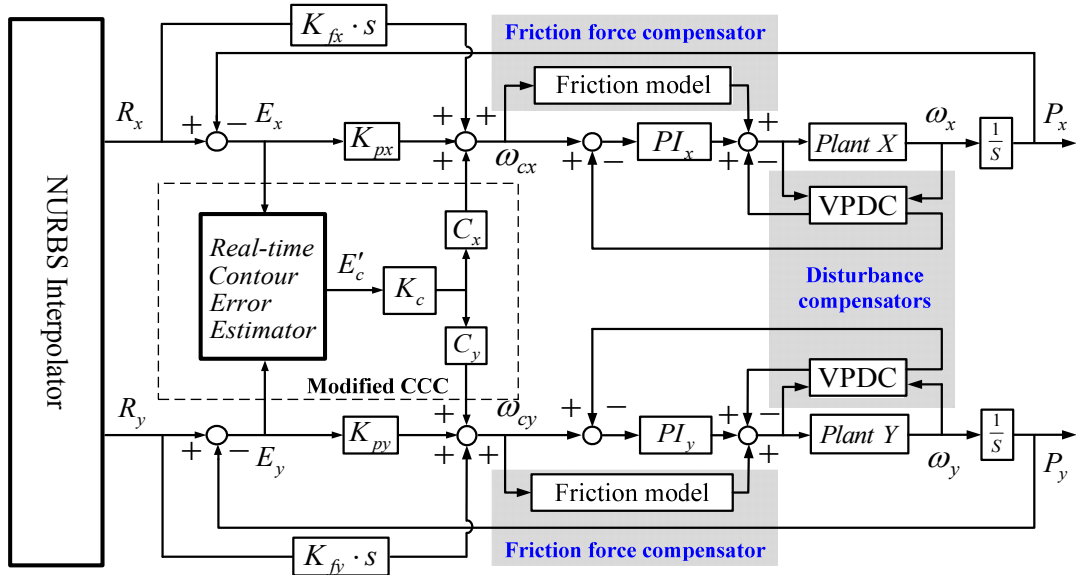
Fig. 5. Schematic diagram of the proposed integrated motion control scheme.
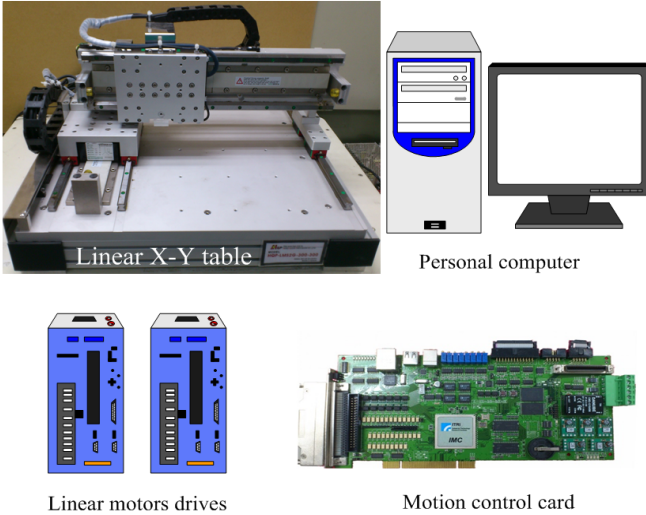

Fig. 6. Hardware of the experimental system used to evaluate the performance of the proposed approach.

$$Fy_{fric}(v)=\begin{cases}1.3\times10^{-3}v+0.5587, & \text{for } v>1\text{mm/s}\\1.1\times10^{-3}v-0.3573, & \text{for } v<-1\text{mm/s}\end{cases} \quad (6)$$

B. Experimental Results

In the experiment, the "Heart-shaped" contour following task is performed (by the linear X-Y table) to verify the effectiveness of the proposed approach. The reference command contour "Heart-shaped" (as shown in Fig. 7) is generated by a NURBS interpolator and its associated parameters are listed in Table II.

Additionally, the contour following task is performed using four kinds of motion control schemes and is tested under two constant feedrate conditions: 60 mm/sec and 30 mm/sec, respectively. The four control schemes used in the experiment are: a P-type tracking controller for individual axis (Kp), a tracking controller combined with a velocity feedforward compensator (Kp+FF), the modified CCC (also combined with a velocity feedforward compensator, CCC+FF), and the proposed integrated motion control scheme. Experimental results are illustrated in Figs. 8-10 and are listed in Tables III and IV.

Figs. 8 and 9 show the comparisons of real contour errors using different motion control structures for feedrate commands 60 mm/sec and 30 mm/sec, respectively. In particular, Fig. 8(a) and Fig 9(a) show the contouring performance using Kp; Fig. 8(b) and Fig 9(b) show the contouring performance using Kp+FF; Fig. 8(c) and Fig 9(c) show the contouring performance using CCC+FF; Fig. 8(d) and Fig 9(d) show the contouring performance using the proposed approach. Table III lists the experimental results, where the performance index "MAX" represents the maximum absolute contour error; "AIAE" represents the average integral of the absolute contour error; and "RMS" represents the root mean square of contour error. Note that the real contour errors shown in Figs. 8-9 and Table III are obtained from an offline calculation.

Fig. 10 illustrates the comparisons of tracking errors among different motion control structures under high feedrate condition (60 mm/sec). Also, the experimental results of tracking errors are listed in Table IV. According to the experimental results shown in Figs 8-10 and Tables III and IV, obviously, the proposed integrated motion control scheme exhibits the best performance among all the tested motion control structures for a free-form contour following task under different feedrate conditions. In particular, when the linear X-Y table is operated in reverse motions, the proposed approach also can cope with the large contour errors occurred due to the inherent friction force or external disturbance.

V. CONCLUSIONS

To further improve contouring accuracy, this paper develops an integrated motion control scheme consisting of two position loop controllers with velocity command feedforward, a modified version of CCC, two friction force compensators, and two disturbance compensators (VPDC).

To test the feasibility of the proposed approach, several free-form contour following experiments have been conducted. Experimental results demonstrate that the proposed approach can significantly reduce the contour and tracking errors for biaxial contour following tasks even in a complex curve contouring operation.
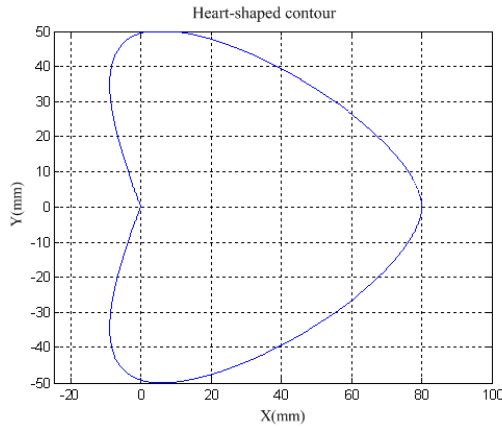

Fig. 7. Reference command trajectory used in the "Hear-shaped" contour following task.
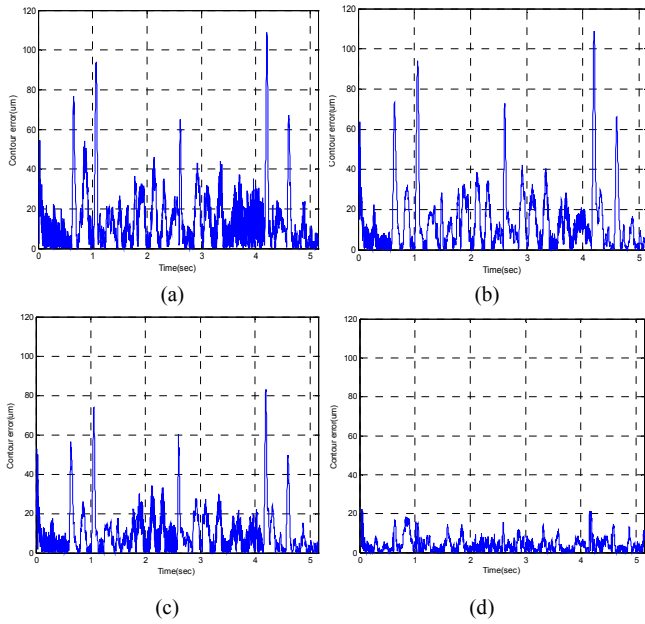

(a)

(b)

(c)

(d)

Fig. 8. Real contour errors of the "Heart-shaped" contour following task for different motion control scheme (60mm/s): (a). Kp; (b). Kp+FF; (c).CCC+FF; (d). the proposed approach.
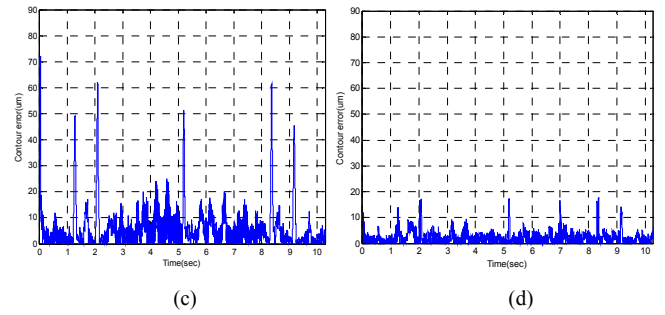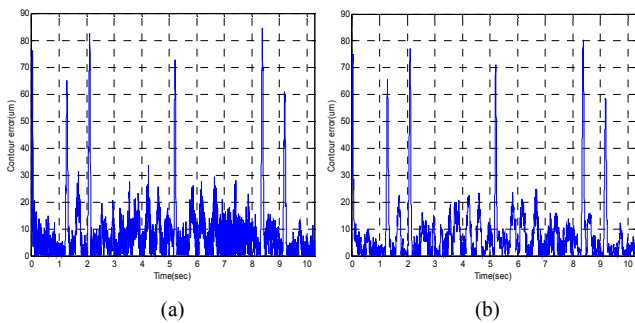

(a)

(b)

(c)

(d)

Fig. 9. Real contour errors of the "Heart-shaped" contour following task for different motion control scheme (30mm/s): (a). Kp; (b). Kp+FF; (c).CCC+FF; (d). the proposed approach.
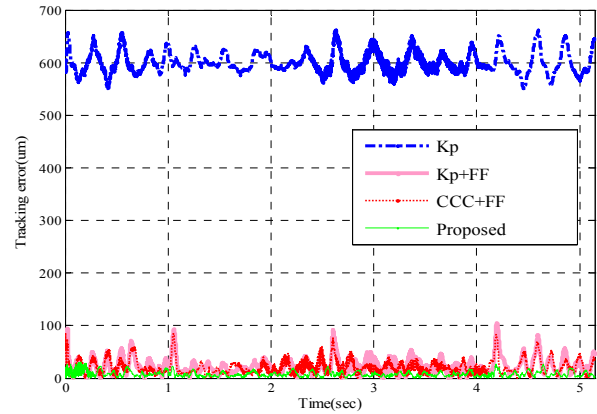

Fig. 10. Tracking errors of the "Heart-shaped" contour following task for different motion control scheme (60mm/s).

REFERENCES

[1] O. Masory, "Improving contouring accuracy of NC/CNC systems with additional velocity feedforward loop," *ASME Journal of Engineering for Industry*, 108 (1986) 227–230.

[2] M. Tomizuka, "Zero phase error tracking algorithm for digital control," *ASME Journal of Dynamic Systems, Measurement, and Control*, 109 (1987) 65-68.

[3] Y. Koren, "Cross-coupled biaxial computer control for manufacturing systems," *ASME Journal of Dynamic Systems, Measurement, and Control*, 102 (1980) 265-272.

[4] K.H. Su, M.Y. Cheng, "Contouring accuracy improvement using cross-coupled control and position error compensator," *International Journal of Machine Tools and Manufacture*, 48 (2008) 1444-1453.

[5] M.Y. Cheng, K.H. Su, S.F. Wang, "Contour error reduction for free-form contour following tasks of biaxial motion control systems," *Robotics and Computer-Integrated Manufacturing*, 25 (2) (2009) 323-333.

[6] Y.S. Tarng, H.Y. Chuang W.T. Hsu, "Intelligent cross-coupled fuzzy feedrate controller design for CNC machine tools based on genetic algorithms," *International Journal of Machine Tools and Manufacture*, 39 (10) (1999) 1673-1692.

[7] Y.T. Shin, C.S. Chen, A.C. Lee, "A novel cross-coupling control design for bi-axis motion," *International Journal of Machine Tools and Manufacture*, 42 (14) (2002) 1539-1548.

[8] M.T. Yan, M.H. Lee, P.L. Yen, "Theory and application of a combined self-tuning adaptive control and cross-coupling control in a retrofit milling machine," *Mechatronics* 15 (2005) 193–211.

[9] S.S. Yeh, Z.H. Tsai, P.L. Hsu, "Applications of integrated motion controllers for precise CNC machines," *International Journal of Advanced Manufacturing Technology*, 44 (2009) 906-920.

[10] M.C. Tsai, I.F. Chiu, M. Y. Cheng, "Design and implementation of command and friction feedforward control for CNC motion controllers," *IEE proceedings, Control Theory and Applications*, 151 (1) (2004) 13-20.

[11] S. Jee; Y. Koren, "A self-organizing fuzzy logic control for friction compensation in feed drives," Proceedings of the American Control Conference, Seattle, Washington, (1995) 205-209.

[12] T. Umeno, T. Hori, "Robust speed control of DC servomotor using modern two degrees-of-freedom controller design," *IEEE Transactions on Industrial Electronics*, 38 (5) (1991) 363-368.

[13] M.T. Yan, Y.J. Shiu, "Theory and application of a combined feedback–feedforward control and disturbance observer in linear motor drive wire-EDM machines," *International Journal of Machine Tools and Manufacture*, 48(3-4) (2008) 388-401.

[14] Z. Jamaludin, H. Van Brussel, J. Swevers, "Friction compensation of an *XY* feed table using friction-model-based feedforward and an inverse-model-based disturbance observer," *IEEE Transactions on Industrial Electronics*, 56 (10) (2009) 3848-3853.

[15] H. S. Lee, M. Tomizuka, "Robust motion controller design for high-accuracy positioning systems," *IEEE Transactions on Industrial Electronics*, 43 (1) (1996) 48-55.

[16] D. Karnopp, "Computer simulation of Slip-Stick friction in mechanical dynamic systems," *ASME Journal of Dynamic Systems*, *Measurement*, *and Control*, 107 (1985) 100-103.

[17] J.C. Wu, K.H. Su, M.Y. Cheng, "Friction and disturbance compensation for speed control of servo control systems," Proceedings of the IECON'10, Nov 07-10, Phoenix, AZ, USA, (2010) 1884-1889.

[18] M.C. Tsai, E. C Tseng, M.Y. Cheng, "Design of a Torque Observer for Detecting Abnormal Load," *Control Engineering Practice*, 8 (2000) 259-269.

[19] M.Y. Cheng, C.C. Lee, "Motion controller design for contour following tasks based on real-time contour error estimation," *IEEE Transactions on Industrial Electronics*, 54 (3) (2007) 1686-1695.

[20] C.T. Johnson, R.D. Lorenz, "Experimental identification of friction and its compensation in precise, position controlled mechanisms," *IEEE Transactions on Industry Applications,* 28 (1992) 1392-1398.

[21] M.Y. Cheng, M.C. Tsai, J.C. Kuo, "Real-time NURBS command generators for CNC servo controllers," *International Journal of Machine Tools and Manufacture*, 42 (7) (2002) 801-813.

TABLE I
PLANT PARAMETERS AND GAIN CONSTANTS USED IN THE EXPERIMENT

Coefficients	Selected parameters	
	X-axis	Y-axis
$\hat{J}_m$ Volt/(mm/s^2)	0.0000974	0.0004615
$\hat{B}_m$ Volt/(mm/s)	0.00090015	0.00105
K_f	1	1
K_P	0.1	0.1
Kv_P	2	2
Kv_I	100	100
K_1	0.05	0.01
K_2	5	5
K_c	0.04	

TABLE II
PARAMETER SETTING OF NURBS CODE FOR THE "HEART-SHAPED" CONTOUR

Order	k=3	
Knot Vector	(0, 0, 0, 0.15, 0.5, 0.5, 0.85, 1, 1, 1)	
Control Point (x, y) mm		Weighting
1	(0.0,0.0)	1.0
2	(-20.0,50.0)	1.0
3	(80.0,50.0)	0.8
4	(80.0,0.0)	5.0
5	(80.0,-50.0)	0.8
6	(-20.0,-50.0)	1.0
7	(0.0,0.0)	1.0

TABLE III
PERFORMANCE EVALUATION OF THE "HEART-SHAPED" CONTOUR FOLLOWING TASK UNDER DIFFERENT FEEDRATE CONDITIONS

Experimental Results / Definitions	Performance index of contour error (μm)		
	MAX	AIAE	RMS
30mm/s			
Kp	84.61	8.48	13.834
Kp+FF	80.44	7.84	13.42
CCC+FF	72.00	6.08	10.30
Proposed	17.89	2.25	3.22
60mm/s			
Kp	108.74	14.60	20.86
Kp+FF	108.75	13.78	20.71
CCC+FF	83.07	10.20	15.31
Proposed	22.23	4.00	5.43

TABLE IV
TRACKING PERFORMANCE COMPARISON AMONG DIFFERENT MOTION CONTROL SCHEMES UNDER HIGH FEEDRATE CONDITION

Experimental Results / Definitions	Performance index of tracking error (μm)		
	MAX	AIAE	RMS
60mm/s			
Kp	662.00	600.09	600.45
Kp+FF	105.00	23.60	28.90
CCC+FF	85.36	21.46	25.96
Proposed	30.50	8.53	10.84